Curvature phase factor in digital holographic microscopy

Ana Doblas[a], Emilio Sánchez-Ortiga[a], Manuel Martínez-Corral[a], Genaro Saavedra[a], Pedro Andres[a], and Jorge Garcia-Sucerquia[a,b,*]

[a]3D Imaging and Display Laboratory, Department of Optics, University of Valencia, E-46100 Burjassot, Spain.

[b]Universidad Nacional de Colombia Sede Medellin, School of Physics, Medellin-050034-Colombia.

ABSTRACT

As digital holographic microscopy (DHM) uses microscope objectives (MO) for enlarging the sample, some associated effects that are not present in optical microscopy have to be considered as quantitative phase imaging (QPI) is regarded. The remaining phase curvature introduced by the MO, which does not affect the optical microscopes, plays a determinant role in the performance of the DHM. In this contribution a thorough analysis of the physical parameters that control the appropriate utilization of MOs in DHM is presented. The analysis is carried for QPI. We study the sample phase perturbations that the MO phase curvature introduces. An analysis of the regular ways as these phase anomalies are removed is presented. The study is supported by means of numerical modeling and experimental results.

Keyword: digital holographic interferometer, quantitative phase imaging, digital processing.

1. INTRODUCTION

Digital holographic microscopy (DHM) allows the numerical reconstruction of a complex wavefield [1-5]. The basic idea is to record the complex amplitude distribution of an object field into an interference pattern with a reference wave from the acquisition of a single digital hologram. As a microscope objective (MO) is used, it appears an additional parabolic phase factor in the object amplitude distribution [6, 7]. This factor affects both phase and amplitude imaging; however, it has a more devastating effect in the hallmark of DHM, namely quantitative phase imaging (QPI). The applications of QPI-DHM are found in different fields, for instance, living cell screening [8-11], particles tracking [12-15] and MEMS evaluation [16-18], hence the correction of such phase curvature is needed.

As QPI-DHM is considered, most of the DHM reported in the literature remove the remaining quadratic phase factor by *a-posteriori* numerical approaches [7, 19, 20] or by recording another hologram without object information [21] or by introducing an identical imaging system on the reference arm [22]. Basically, these digital processes involve the knowledge of the center and radius of the curvature phase factor to compensate its effects on QPI-DHM. However, even minimum errors in these parameters perturb the accuracy of the measurement [23].

To overcome this drawback, a telecentric imaging system is utilized. In this case, the parabolic phase factor is eliminated physically and the system has the property of being shift-invariant [23], in contrast of the usual arrangement. Our goal in this work is to present a thorough analysis of a physical performance of a QPI-DHM configuration to evaluate the performance of the imaging system in the set-up.

The paper is organized as follows. In Section 2, we explain the basic theory of a DHM and derive the equations that describe the imaging system. In Section 3, we analyze the inaccuracies introduced by the MO when imaging system is non-telecentric and telecentric. Computer modeling and experimental verifications are shown. Finally, in Section 4, we summarize the main achievements of our research.

2. THEORY

The basic architecture of a transmission DHM (see Figure 1) is a modified Mach-Zenhder interferometer where the light comes from a He-Ne laser of wavelength $\lambda = 633$ nm. In this study, we utilize a plane reference wave. The wavefield scattered by the specimen is collected by a microscope objective MO (infinity-corrected), and the object

*jigarcia@unal.edu.co; phone +34 963544078

8th Iberoamerican Optics Meeting and 11th Latin American Meeting on Optics, Lasers, and Applications,
edited by Manuel Filipe P. C. Martins Costa, Proc. of SPIE Vol. 8785, 87856Q
 · doi: 10.1117/12.2026176

image is formed by the tube lens TL, whose focal length is f_{TL} , at the image plane (IP). The holograms are recorded on a charge-couple device (CCD) with 1024x1024 square pixels of 6.9 μm side.

To achieve an off-axis configuration, both the beam-splitter BS2 and the mirror M2, which reflect the reference wave *R*, are slightly tilted such as the reference wavefield interferes with the object wave *O*

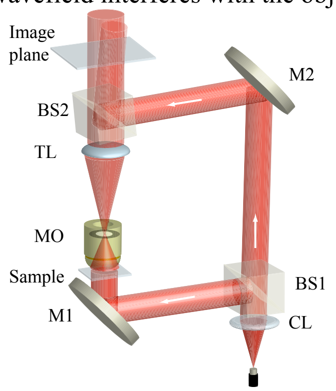

Figure 1: Scheme of the transmission DHM for evaluating the accuracy of the QPI-DHM. CL is a collimating lens; BS1 and BS2 are beam-splitter cubes; M1 and M2 are mirrors; MO is a microscope objective; and, TL is a tube lens.

with a small angle θ. At the CCD plane, the interference between the object wave and the reference wave produces the hologram intensity

$$I(x,y)=|R|^2+|O|^2+RO^*+R^*O, \tag{1}$$

being (x,y) the spatial transverse coordinates, $|\ |^2$ the square modulus and $*$ the complex conjugate operation. The two first terms are the zero-order of diffraction and the other two are the virtual and real terms, respectively also known as twin images.

To reconstruct the real image $O(x,y)$, the two-dimensional Fourier transform of Eq. (1) is calculated. In the corresponding spatial spectra, the spatial frequencies of the zero-order term are placed in the center. Whereas that the frequencies of the other terms are located symmetrically with respect to the center of the image [24]. The distance between one of these terms and the zero-order term can be measured and is directly related with the incidence angle θ. The Fourier transform image is spatial filtered out to eliminate the zero-order and the twin contributions. As the term that contains the real image, R^*O, is a product between the complex conjugate reference wave and the object wave, it is necessary to multiply with a numerical version of the reference wave such as

$$\Psi(m,n)=R_N R^*O, \tag{2}$$

where (m,n) are integers and

$$R_N(m,n)=\exp\left[i\frac{2\pi}{\lambda}\left(k_x m\Delta x+k_y n\Delta y\right)\right], \tag{3}$$

being $(\Delta x,\Delta y)$ pixel size of the CCD camera and (k_x,k_y) can be measured directly in the Fourier spectra.

Since $\Psi(m,n)$ is an array of complex numbers, it is possible to obtain the amplitude-contrast image

$$A(m,n)=\sqrt{\mathrm{Re}\left[\Psi(m,n)\right]^2+\mathrm{Im}\left[\Psi(m,n)\right]^2}, \tag{4}$$

and the phase-contrast image

$$\phi(m,n)=\arctan\left[\frac{\mathrm{Im}\left[\Psi(m,n)\right]}{\mathrm{Re}\left[\Psi(m,n)\right]}\right]. \tag{5}$$

It is assumed that the sample introduces only a phase delay $\phi(m,n)$ resulting from a difference of refractive index, $(n-n_0)$, and/or thickness, e. These parameters are correlated by the following expression $\phi={}^{2\pi}\!/_{\lambda}(n-n_0)e$.

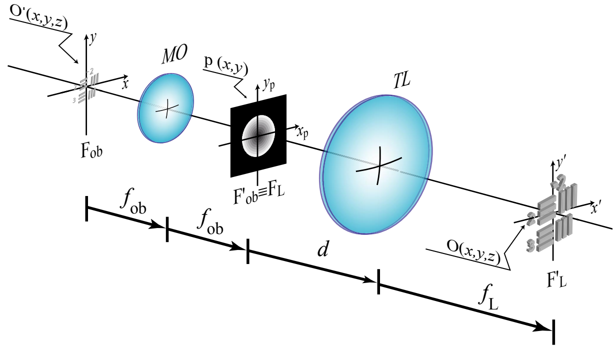

Figure 2: Illustration of the geometry of the object arm.

As shown in Figure 1, the optical scheme in the object arm is a simple imaging system. A zoom of this arrangement is illustrated in Figure 2. Depending on the distance between the MO and TL, it is possible to achieve a telecentric or non-telecentric arrangement. Following regular imaging ABCD transformations [25, 26] and after straightforward algebra, the expression of the complex wavefield produced by the imaging system at the CCD plane is given by

$$O(x,y) = -\frac{1}{M}\exp\left[i2\pi\frac{f_{MO}+d+f_{TL}}{\lambda}\right]\exp\left[i\frac{\pi}{\lambda C}\left(x^2+y^2\right)\right]\left\{O'\left(\frac{x}{M},\frac{y}{M}\right)\otimes_2\tilde{p}\left(\frac{x}{\lambda f_{TL}},\frac{y}{\lambda f_{TL}}\right)\right\}, \qquad (6)$$

where $M=-f_{TL}/f_{MO}$ is the magnification of the imaging system and $\otimes_2$ represents the 2D convolution between the complex amplitude $O'(\ )$ scattered by the object and the Fourier transform of the aperture function of the imaging system. At this point it is important to note the presence of a quadratic phase factor $\exp\left[i\pi/\lambda C\left(x^2+y^2\right)\right]$ [6, 7, 23] associated with the use of the MO. The radius of curvature C of this parabolic phase factor is given by

$$C = \frac{f_{TL}^2}{f_{TL}-d}, \qquad (7)$$

where d is the distance between the MO aperture stop and the TL plane, see Figure 2.
As a direct consequence of this quadratic phase term, the imaging system is shift-variant [23, 27]. Generally, the majority of DHMs work in a non-telecentric arrangement, thus the measurement of the QPI-DHM depends on the object position. However, it is possible to remove fully this quadratic phase factor by using a telecentric configuration, namely $d=f_{TL}$ [28]. Contrary to what happens in the general case, $d\neq f_{TL}$, now the imaging system has the shift-invariant property.

3. Quantitative phase imaging: numerical and experimental results

Our aim is to show the effect of the quadratic phase factor on phase measurements. To do that, the experimental set-up has been modeled numerically. By using Eqs. (1) and (6) to generate synthetic hologram, we imaged a phase object composed by two identical disks with radius 639 µm; each disk has a phase jump of 1.7 rad. The disks have their centers separated 2.534 mm to cover the half of field of view (FOV).
In our study, the variation of a parameter called offset, $\left|f_{TL}-d\right|$, allows the DHM operates in the telecentric or non-telecentric regimen.
To simulate the most ideal case of the numerical correction of the quadratic phase factor, we have assumed a shift of one-pixel on-one-thousand on the location of the center and an error of 2% on the radius of curvature. Figure 3 shows a three-dimensional perspective of the reconstructed phase distribution for both configurations. The measured phase of the object is plotted along a straight line connecting the centers of the disks (see Figure 3). For both cases, telecentric and non-telecentric, the measured phases for the disk placed at the very center the FOV are almost identical; minimum\maximum variations of the 2.7\6.7 % for an offset of 40 mm are observed with respect to the zero offset (telecentric case). However when the phase object is placed at the edge of the FOV, the minimum\maximum variations become more significant, are the order of 31.4\70.8% with respect to the zero offset. These findings are summarized in Figure 4.

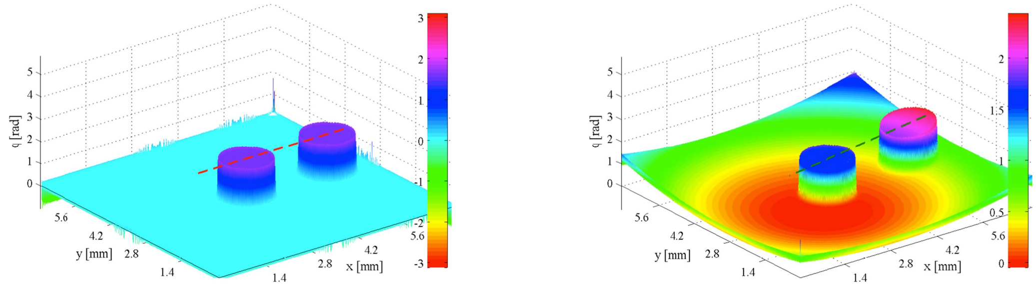

(a) (b)

Figure 3. Three-dimensional perspective of the modeling phase object for (a) the telecentric arrangement and (b) the non-telecentric arrangement with an offset of 40 mm.

The inaccuracies described above can be tested experimentally using the system illustrated in Figure 1. The experiment has been made with a diffractive Fresnel lens as a phase object. The object shows a phase jump of 1.87 rad when the source's wavelength is 633 nm. The scattered distribution of the Fresnel lens is collected by a MO 4×/0.25 and the focal length of the TL is 200 mm.

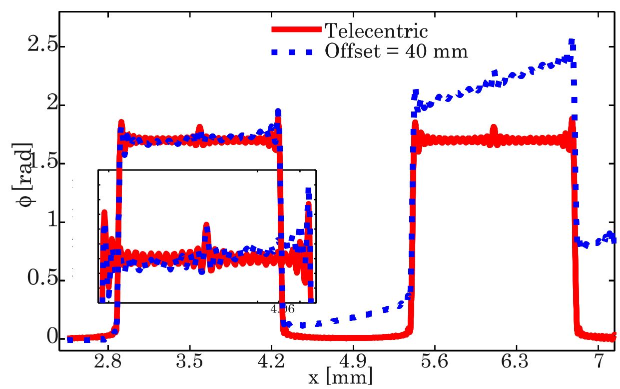

Figure 4. Phase profiles along the lines drawn in Figure 3 for different values of the offset in the imaging system. The solid\dotted line corresponds to 0\40 mm offset. The inset shows that even at the center of the FOV, the non-telecentric configuration introduces variations on the measured phase.

To evaluate the accuracy of the QPI-DHM, the Fresnel lens is imaged at the very center of the FOV and at the edge of it, for different values of the offset of the imaging system. All holograms have been post processed carefully. For the telecentric geometry, reconstructed phase distributions, Figure 5, are only obtained through a spatial filtering to eliminate the three first terms of Eq. (1) and the correction of the reference wave, whose parameters $\left(k_x, k_y\right)$ are, respectively, 1.5739 and 1.7027 radians.

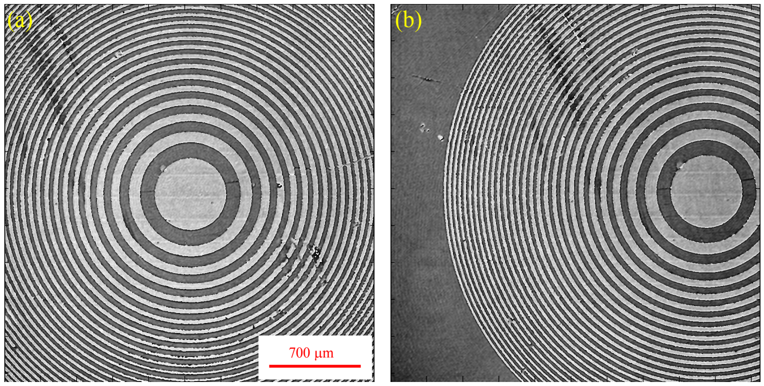

Figure 5. Digital holograms recorded by the CCD when the Fresnel lens is at the (a) center and (b) edge of the FOV; (c, d) the corresponding spectra; (e, f) filtered two-dimensional Fourier spectrum and (g, h) wrapping reconstructed phase distribution.

For the non-telecentric imaging system, the suppression of the remaining quadratic phase factor is corrected by fitting polynomial curves along selected profiles extracted from the area of the wrapped reconstructed phase distribution where it is assumed the sample is constant [29]. It is interesting to mention that curve-fitting is applied on unwrapped images. After the parabolic wavefront correction, the reconstructed phase images are shown in Figure 6. We can compare these reconstructions with the ones obtained from the telecentric DHM. Clearly, the images corresponding to the telecentric case are visually better, without the appearance of digital noise.

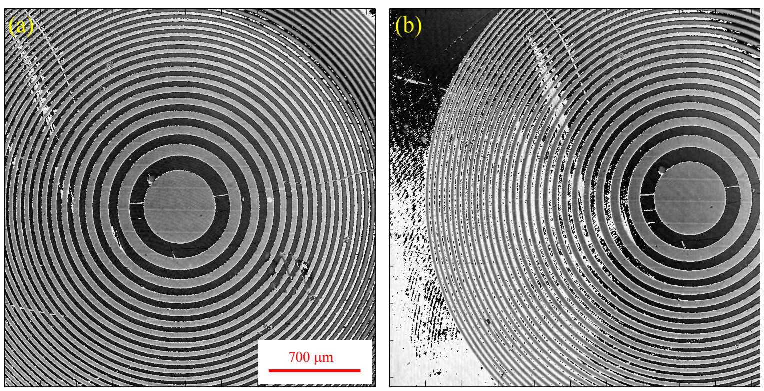

Figure 6. (a, b) Reconstructed phase map of the Fresnel lens for a non-telecentric geometry and after correcting the spherical factor.

Finally, from Figures 5 and 6, we plot the phase profiles of the Fresnel lens at the two studied positions on the FOV and for the two studied configurations, see Figure 7.For the telecentric imaging system, the measured phase does not change; for both positions of the object we measure an average phase jump of 1.74±0.25. Nevertheless, for an offset of 40 mm, the phase measurement shows a clear variation with respect to the telecentric measurement. We can see the same upward behavior at the edge of the FOV between the experimental result and the one modeling (Fig. 4). The difference between the measured phase for the same object at the very center and at the edge of the FOV is of the order of 19.8%. Whereas that for the case of the telecentric geometry this difference is 1.74%.

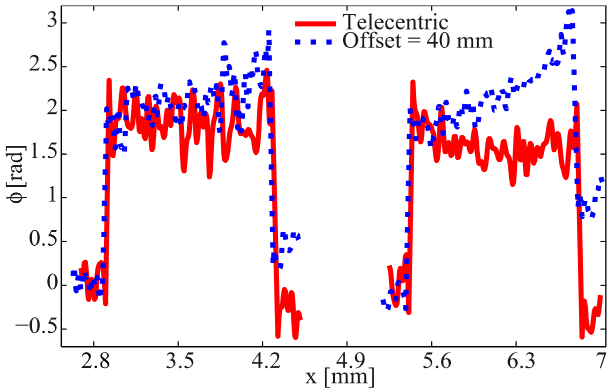

Figure 7. Experimental profiles of the Fresnel lens placed at different positions on the FOV, as the imaging system has different offsets; solid\dotted line for 0\40mm offset.

4. CONCLUSIONS

In conclusion, we have shown the inaccuracies of the QPI-DHM measurement by using a non-telecentric imaging system. The use of a non-telecentric arrangement provides a shift variant system. This property perturbs QPI-DHM measurements of identical objects placed at different positions on the FOV. The experimental results agree with the numerical modeling. In both, the phase measurement is clearly different for a non-telecentric geometry with respect to the telecentric arrangement. By contrast, when the imaging system is telecentric, QPI-DHM measurements have no dependence on the specimen position and this feature makes it very useful as a tool for measuring in life and material sciences.

ACKNOWLEDGMENTS

Financial support by the Ministerio de Economia y Competitividad, Spain (Grant DPI2012-32994) and the GeneralitatValenciana (Grant PROMETEO2009-077) is gratefully acknowledged. A. Doblas greets funding from the University of Valencia through the predoctoral fellowship program “Atracció de Talent”. J. Garcia-Sucerquia gratefully acknowledges the financial support from the Universidad de Valencia, Spain, under the Program “Estancias Temporales para Investigadores Invitados",Colciencias grant number 110205024 and UNAL grants numbers 110201003 and 110201004.

REFERENCES

1. M. K. Kim, “Principles and techniques of digital holographic microscopy,” SPIE Reviews **1**, 018005 (2010). doi: 10.111716.0000006.
2. P. Picart, and J.-C. Li, *Digital Holography*, Wiley (2012). ISBN-13: 978-1848213441
3. T. Kreis, *Handbook of Holographic Interferometry: Optical and Digital Methods*, Wiley (2004). ISBN 3-527-40546-1.
4. G. Popescu, *Quantitative phase imaging of cells and tissues*, McGraw-Hill, New York, 2011.
5. E. Cuche, F. Bevilacqua, and C. Depeursinge, "Digital holography for quantitative phase-contrast imaging," Opt. Lett. 24, 291-293 (1999).
6. E. Cuche, P. Marquet, and C. Depeursinge, "Simultaneous amplitude-contrast and quantitative phase-contrast microscopy by numerical reconstruction of Fresnel off-axis holograms," Appl. Opt. **38**, 6994-7001 (1999).
7. T. Colomb, F. Montfort, J. Kühn, N. Aspert, E. Cuche, A. Marian, F. Charrière, S. Bourquin, P. Marquet, and C. Depeursinge, "Numerical parametric lens for shifting, magnification, and complete aberration compensation in digital holographic microscopy," J. Opt. Soc. Am. A **23**, 3177-3190 (2006).
8. B. Kemper, D. Carl, J. Schnekenburger, I. Bredebusch, M. Schäfer, W. Domschke, and G. von Bally, “Investigation on living pancreas tumor cells by digital holographic microscopy,” Journal of Biomedical Optics **11**, 034005 (2006).
9. N. Pavillon, J. Kühn, C. Moratal, P. Jourdain, C. Depeursinge, P. J. Magistretti, and P. Marquet, “Early cell death detection with digital holographic microscopy,” PLoS ONE **7**, e30912 (2012).

10. J. Kühn, E. Shaffer, J. Mena, B. Breton, J. Parent, B. Rappaz, M. Chambon, Y. Emery, P. Magistretti, C. Depeursinge, P. Marquet, and G. Turcatti, "Label-free cytotoxicity screening assay by digital holographic microscopy," Assay and Drug Development Technologies **19**, 101-107 (2013). doi: 10.1089/adt.2012.476.
11. M. Puthia, P. Storm, A. Nadeem, S. Hsiung, and C. Svanborg, "Prevention and treatment of colon cancer by peropal administration of HAMLET (human α-lactalbumin made lethal to tumour cells)," Gut **0**, 1-12 (2013).
12. N. Warnasooriya, F. Joud, P. Bun, G. Tessier, M. Coppey-Moisan, P. Desbiolles, M. Atlan, M. Abboud, amd M. Gross, "Imaging gold particles in living cell envioronments using heterodyne digital holographic microscopy," Optics Express **18**, 3264-3273 (2010).
13. B. Kemper, A. Bauwens, A. Vollmer, S. Ketelhut, P. Langehanenberg, J. Mütihng, H. Karch, and G. von Bally, "Label-free quantitative cell division monitoring of endothelial cells by digital holographic microscopy," Journal of Biomedical Optics **15**, 036009 (2010).
14. H. Sun, B. Song, H. Dong, B. Reid, M. A. Player, J. Watson, and M. Zhao, "Visualization of fast-moving cells in vivo using digital video microscopy," Journal of Biomedical Optics **13**, 014007 (2008). doi:10.1117/1.2841050
15. C. J. Mann, L. Yu, and M. K. Kim, "Movies of cellular and sub-cellular motion by digital holographic microscopy," Biomedical Engineering Online **5**, 1-10 (2006). doi: 10.1186/1475-925X-5-21.
16. Y. Emery, E. Solanas, N. Aspert, A. Michalska, J. Parent, and E. Cuche, "MEMS and MOEMS resonant frequencies analysis by digital holography microscopy (DHM)," Proceeding of SPIE **8614**, 86140A (2013). doi: 10.1117/12.2009221.
17. A. Asundi, *Digital Holography for MEMS and Microsysyem Metrology*, Wiley (2011).
18. G. Coppola, S. De Nicola, P. Ferraro, A. Finizio, S. Grilli, M. Iodica, C. Magno, and G. Pierattini, "Characterization of MEMS structures by microscopic digital holography," Proceedings of SPIE **4945**, 71 (2003).
19. T. Colomb, J. Kühn, F. Charrière, C. Depeursinge, P. Marquet, and N. Aspert, "Total aberrations compensation in digital holographic microscopy with a reference conjugated hologram," Opt. Express **14**, 4300-4306 (2006).
20. K. W. Seo, Y. S. Choi, E. S. Seo, and S. J. Lee, "Aberration compensation for objective phase curvature in phase holographic microscopy," Opt. Lett. **37**, 4976-4978 (2012).
21. P. Ferraro, S. De Nicola, A. Finizio, G. Coppola, S. Grilli, C. Magro, and G. Pierattini, "Compensation of the Inherent Wave Front Curvature in Digital Holographic Coherent Microscopy for Quantitative Phase-Contrast Imaging," Appl. Opt. **42**, 1938-1946 (2003).
22. C. Mann, L. Yu, C.-M. Lo, and M. Kim, "High-resolution quantitative phase-contrast microscopy by digital holography," Opt. Express **13**, 8693-8698 (2005).
23. A. Doblas, E. Sánchez-Ortiga, M. Martínez-Corral, G. Saavedra, P. Andrés, and J. Garcia-Sucerquia, "Shift-variant digital holographic microscopy: inaccuracies in quantitative phase imaging," Optics Letters **38**, 1352-1354 (2013).
24. E. Cuche, P. Marquet, and C. Depeursinge, "Spatial Filtering for Zero-Order and Twin-Image Elimination in Digital Off-Axis Holography," Appl. Opt. **39**, 4070-4075 (2000).
25. D. S. Goodman, "General Principles of geometric optics," in *Handbook of Optics*, M. Bass, eds. (McGraw-Hill, New York, 1995).
26. S. A. Collins, "Lens-system diffraction integral written in terms of matrix optics," J. Opt. Soc. Am **60**, 1168-1179 (1970).
27. D. P. Kelly, B. M. Hennelly, N. Pandey, T. J. Naughton, and W. T. Rhodes, "Resolution limits in practical digital holographic systems," Optical Engineering **48**, 095801-095801 (2009).
28. E. Sánchez-Ortiga, P. Ferraro, M. Martínez-Corral, G. Saavedra, and A. Doblas, "Digital holographic microscopy with pure-optical spherical phase compensation," J. Opt. Soc. Am. A **28**, 1410-1417 (2011).
29. T. Colomb, E. Cuche, F. Charrière, J. Kühn, N. Aspert, F. Montfort, P. Marquet, and C. Depeursinge, "Automatic procedure for aberration compensation in digital holographic microscopy and applications to specimen shape compensation," Appl. Opt. **45**, 851-863 (2006).